JOURNAL REVIEW

Microfluidic Modeling and Design for Continuous Flow in Electrokinetic Mixing-Reaction Channels

Xiang He and Steinar Hauan
Dept. of Chemical Engineering, Carnegie Mellon University, 5000 Forbes Avenue, Pittsburgh, PA 15213

DOI 10.1002/aic.10985
Published online September 28, 2006 in Wiley InterScience (www.interscience.wiley.com).

Advances in microfluidics have inspired novel designs of LoC systems with integrated functionality and improved thermal and mass-transfer characteristics. As important functional subsystems of LoC, microfluidic reaction systems can significantly reduce the need for space, materials, and energy, and often have shorter response times. Iterative design studies require accurate and fast models for subsystems. Here, we present two PFR-network-based models and a method of lines model for reaction subsystems. These two models employ two different discretization methods to reduce the set of PDEs into a system of coupled ODEs. We use our model to analyze an example micro mixing-reaction system. The results illustrate how reaction channel length and the electric potential difference influence the product yields and selectivities. These models are ready to be combined other subsystem models for the design of integrated LoC systems. © 2006 American Institute of Chemical Engineers *AIChE J,* 52: 3842–3851, 2006
Keywords: lab-on-a-chip design, microscale reactors, reduced order models

Introduction

Micrototal analysis systems (μTAS), also known as "Lab-on-a-Chip,"[1] are terms used to connote the miniaturization of chemical, biological and biochemical analysis devices.[2,3] A Lab-on-a-Chip (LoC) system is a microfluidic device that mimics the functions of a standard analytical chemistry laboratory: sample preparation, mixing, reaction, injection, separation, and detection.[3] Miniaturization provides LoC devices with some key benefits: the drastic reduction of reagent consumption, which translates to cost savings; integration, which offers the advantages of faster analysis and sometimes novel, synergistic capabilities that may not be attainable otherwise; automation, that allows more precise and reproducible operations resulting in higher data quality.[2] LoC systems have various applications in clinical diagnosis, such as analysis of drugs in biological fluids,[4] DNA separation and detection,[5] and immunoassay.[6] A LoC device can also be used for countering bioterrorism threats and is typically capable of performing sampling and real time testing of samples for biochemical toxins.[7] There exist a large variety of LoC devices that differ in their functional tasks, as well as detection methods. Consequently, using a library of generic LoC designs for all applications may either fail for some analytical procedures or be over designed as for performances, costs and chip size. To avoid these problems, a design methodology is needed to make it easy to customize LoC devices according to applications.

LoC design

While the advantages of microfluidic systems have been demonstrated,[8] systematic design methods are only begun to emerge.[7,9,10] Most often, to design a LoC device with optimized geometry and performance, the designer is reduced to using trial-and-error approaches that involve a large number of experimental tests and long development cycles. This deficiency becomes even more acute when large-scale microfluidic integration is needed.[11] Our long term goal is to develop a fast, robust, and accurate design methodology for integrated and multiplexed microfluidic systems. This general methodology will accelerate the design and customization of LoC devices for specific applications. In our approach to automated LoC design, the inner loop, that is, the evaluation of a particular layout instance of the unit operation, must be solved a large number of times; the typical place-and-route algorithms from integrated circuit design take on the order of ten to hundred thousand

Correspondence concerning this article should be addressed to X. He at xiangh@andrew.cmu.edu

iterations. It is, thus, computationally intractable to even think about approaches where the evaluation of single unit operations are measured in minutes.

In LoC devices, the subsystem design and ultimate chip layout are intimately linked due to the influence that channel geometry has on device performance.[9] The different operations of a LoC requires modules for subsystems: mixing, reaction, injection, and separation. Several component modules have already been developed:[12] a passive micromixer model that is represented by a system of mixing elements of simple geometry;[13] an electrophoretic separation channel simulator that employs accurate algebraic physical models;[14] and a functional injector model based on neural-network.[15] So far, there is no parametrized module to deal with the microscale steady-state mixing-reaction subsystems. While a coarse-grid set of *a priori* FEM simulations could be envisioned when solving this problem, it would be nonobvious to know the geometric layout of each section upfront and, thus, search the correct parameters. In fact, there is a large body of literature, in particular for separation subsystems, that describe the detailed link between irregularities in concentration profiles, and the device geometry.[16,17] Coupled with the need for highly accurate results, not only for geometry, but also for different flow and reaction regimes, the simulation database would have to be enormous to cover all the relevant cases visited by a place-and-route approach. This article addresses the need to develop a mixing-reaction module in the LoC library, which is stable, accurate, and fast.

Microreactor design

Microreactors are important functional units for LoC devices. They can also work as independent chemical reaction devices. They have several advantages brought by miniaturization:[8,18,19] (a) The increased surface to volume ratio of microreactors improves heat and mass-transfer rates by at least one-order of magnitude, which allows reactions to be performed under more aggressive conditions with higher yields than can be achieved with conventional reactors; (b) In addition, slow-batch processes caused by slow mass and heat transfer can be replaced by continuous flow processes in microreactors; (c) The inherent safety characteristics suggest that microreactors should enable distributed point-of-use synthesis of chemicals with storage and shipping limitations, such as highly reactive and toxic intermediates.

Much of the current research on microfluidic reaction systems is centered on the fabrication of microreactors for experimentation. Ehrfeld et al.[8] presented an overview of the manufacturing techniques that covered the fabrication of micromixers, microreactors, and micro-heat exchangers. Jensen et al.[20] created a hydrodynamically pumped cross-flow microreactor and demonstrated the potential of it as a laboratory tool for heterogeneous catalyst testing. Haswell et al.[21] considered electrokinetic based fluidic pumping systems. They described the fundamental characteristics and emerging applications of microreactors in the field of synthetic chemistry.[19,22] Modeling of microscale reactors has also been found in the literature. Vlachos et al.[23] used a Monte Carlo algorithm to model the induction times in ignition of spatially homogeneous hydrogen and air mixtures in finite size microreactors. They examined the effect of reactor size on induction time for different reaction conditions. Chatterjee et al.[24] developed a reactor model represented by a set of ordinary differential equations, and solved by a trapezoidal scheme. Multiple authors[21,25,26] developed models for single and multiple segmented flows in microreactors where diffusion and reaction only took place at the leading and ending edges of the segments. Although these models properly simulate and analyze certain reactive fluid behavior in small geometries, they either are batch-reactor models with the assumption that species achieve perfect mixing prior to the start of reaction or require complicated injection methods before the reactor to produce a special type of segmented flow.

This article presents two reduced order models for electrokinetic continuous-flow microreactors. The models can take any concentration profile of reactants at the reactor inlets and simulate diffusion, convection, and reaction inside of reaction channels of any length. We present two approaches that both reduce the set of partial-differential equations (PDEs) to a system of coupled ordinary-differential equations (ODEs). Our first approach is based on physical insights and consists of approximating the reactive channels by a series of interconnected parallel plug flow reactors (PFR). The second approach is based on mathematical simplification of the underlying equations. By using the method of lines (MOL), the spatial derivatives for the diffusional mixing in reaction channels are approximated by finite difference relationships. These models are verified by numerical simulations in COMSOL, a finite element solver. These models are order of magnitude faster than COMSOL, and, therefore, allow parametric studies of a particular microreactor, as well as enable integration into total LoC synthesis and layout approaches.[27]

This article is organized as follows: The Background section introduces the governing equations for the systems that we are interested in and describes dimensionless parameters that are important for the reactor design; The Model development section presents the discretization methods used to solve the governing equations; The Model Analysis section discusses the sensitivity study of the dimensionless parameters that affect product yields and selectivities; The Example Results section discusses some example results, which shows the usage of our model for microreactor design; The Conclusion presents conclusions to microreactor models.

Background

The fabrication of LoC devices is typically done on glass or plastic substrates with techniques adapted from the semiconductor industry. Figure 1 shows our canonical view of a LoC device. This single chip has several unit operations: mixing, reaction, injection, separation, and detection. In this article, we will limit our focus to flow units with simultaneous reaction and mixing.

The fluidic transport in microreactors can be driven by an electric field[6,21] or a pressure gradient.[18,20,28] This article focuses on the electrokinetic pumping reactor to be consistent with our separation model[14] that based on electrophoretic separation. In electrokinetic based pumping systems, the method for driving fluid motion is electroosmosis.[29] When an electric field is applied to a fluid in an insulating channel, the equilibrium electrical double layer is generated adjacent to the channel wall. Inside the double layer, the velocity and chemical reac-

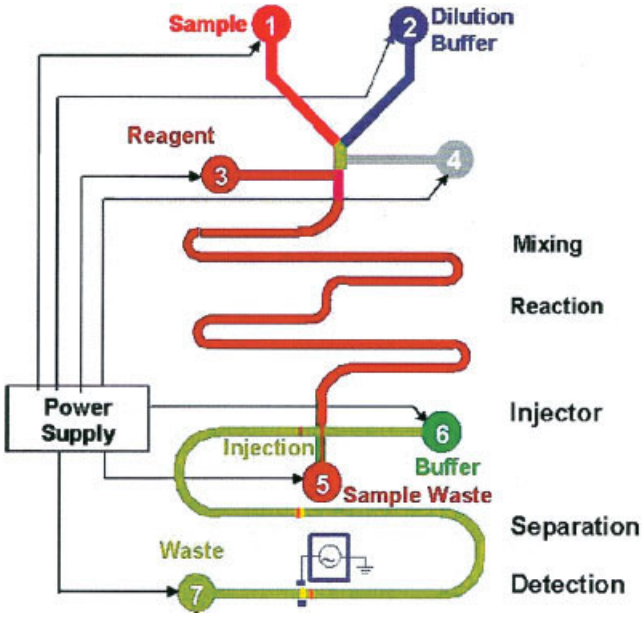

Figure 1. Canonical Lab-on-a-chip with subsystems: mixing, reaction, injection, separation, and detection.

[Color figure can be viewed in the online issue, which is available at www.interscience.wiley.com.]

tion rates are zeros.[30] As the thickness of the double layer is normally small compare to the channel width, we only need to consider the region outside of the double layer, where the fluid has a uniform velocity and nonzero reaction rates. The resulting electroosmotic velocity v_{eo} is given by

$$v_{eo} = \mu_{eo} E \tag{1}$$

where μ_{eo} is the transport mobility due to electroosmotic flow, and E is the applied electric field. In this fluidic system, the charged species are under the influence of an electric field, which results in the electrophoretic velocity

$$v_{ep} = \mu_{ep} E \tag{2}$$

where μ_{ep} is the electrophoretic mobility. The total migration velocity v of species is the sum of both the electrophoretic v_{ep}, and the electroosmotic v_{eo} transport velocities[31,32]

$$v = v_{ep} + v_{eo} = (\mu_{ep} + \mu_{eo})\, E \tag{3}$$

μ_{ep} is a property of species, which is a function of the net charge and the hydrodynamic radius of the species.[31] Species with different charges and different hydrodynamic radius will have different μ_{ep}. This results in the difference of the total migration velocity v between species. This velocity difference is the basis for the electrophoretic separation that is considered in our separation model.[14] In our microfluidic mixing-reaction systems, we are considering steady state homogeneous reaction problems. The difference between the flow rates of species will affect the relative amount of reactants and products presented in the microreactor. As a result, it will have an influence on the

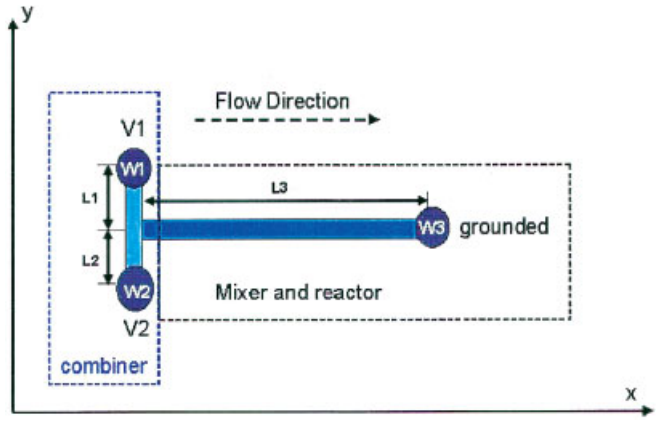

Figure 2. Illustration of a basic micromixing and reaction system.

[Color figure can be viewed in the online issue, which is available at www.interscience.wiley.com.]

reaction equilibrium and the speed for the reaction to reach this equilibrium. This effect is captured by the convection term in the following PDE.

In a microfluidic mixing-reaction system, the concentration change is caused by convection, diffusion, and reaction[29,33]

$$\frac{\partial c_i}{\partial t} = D_i \nabla^2 c_i - v_i \cdot \nabla c_i + r_i \qquad i = 1, \ldots, NC \tag{4}$$

where D_i is the diffusivity, c_i the concentration, and r_i the reaction term related to species i, and NC is the number of components. We will make use of two dimensionless (2D) numbers for classifying the behavior of microfluidic systems. The Peclet number (Pe_i) is the ratio of convective to diffusive mass transport for species i in a fluid, $Pe_i = (v_i l/D_i)$, where l is the system characteristic length, v_i the fluid velocity, and D_i the diffusivity for species i. If Pe_i is large, convection dominates mass transport; if Pe_i is small, diffusion dominates mass transport. The Damkohler number (Da_i) known from classical reactor analysis[34] represents the ratio of characteristic time for convection, and the time for chemical reaction for species i, $Da_i = (t_{cov,i}/t_{rxn,i})$. If Da_i is large, the overall system behavior is dominated by reaction; if Da_i is small, convective mass transport dominates the system. The Damkohler number describes the degree of conversion that can be achieved in a continuous flow reaction system.

Figure 2 shows a simple micro-mixing-reaction system. This system contains three connected reservoirs, each containing an electrode used to create an electric potential gradient. In the reaction channel, the fluid driven by electric field only flows in the x direction and the species' velocity profiles across the channel are flat except close to the channel wall.[32,35] Since the species are not always perfectly mixed before entering the reaction channel, their concentrations may vary in both the x direction, and the orthogonal y direction across the channel. The low Reynolds number operation of microscale flows[25] indicates that mixing in the y direction is caused by diffusion only. The convection term in the y direction from the original PDE can be neglected. In a typically designed microfluidic system, the fluid flows fast enough that the concentration

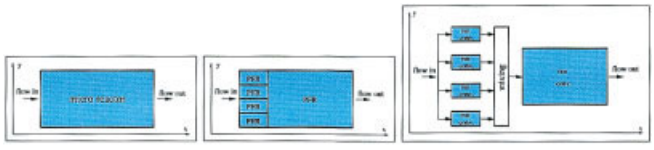

Figure 3. The microreactor is represented by a PFR combination model. The calculations are carried out sequentially: (1) reaction and convection in the column of PFR in parallel, (2) complete mixing of the streams coming out from the parallel PFRs, (3) reaction and convection in the full width PFR.

[Color figure can be viewed in the online issue, which is available at www.interscience.wiley.com.]

changes caused by diffusion in the x direction is much less than those caused by convection. In channel based microreactors, it is safe to only consider convection in the x direction. We further assume that all diffusion coefficients are independent of concentration and that all thermal effects are negligible. For a steady-state case, Eq. 4 can be rewritten as

$$v_{i,x}\frac{\partial c_i}{\partial x} = D_i\left(\frac{\partial^2 c_i}{\partial y^2}\right) + r_i \qquad i = 1, \ldots, NC \tag{5}$$

Our microreactor models are based on this set of PDEs. This article presents two different approaches that approximate this PDE system as an ODE system, which is easier to solve and normally has shorter computational time.

Model Development

Physical Models

In our microfluidic system, the fluid has a pluglike velocity profile. When modeling this system, it is natural to base the model on the classic plug flow reactor (PFR). The design equation for a PFR is

$$\frac{dF_i}{dV} = r_i \tag{6}$$

where V is the reactor volume, F_i the flow rate, and r_i the reaction rate of ith species. When the fluid velocity is constant, the design equation can be rewritten as

$$v_{i,x}\frac{dc_i}{dx} = r_i \tag{7}$$

where c_i is the concentration, and v_{ix} the velocity of ith species in the x direction. Compare this new design equation with Eq. 5, we can see that it lacks the diffusion term, since a PFR assumes a uniform inlet concentration, and, thus, do not consider axial diffusion. However, in our system the inlet-concentration distributions are not necessarily uniform, but depend on injection methods, and the degree of mixing before the reactor. If we use one PFR to model our system, we have to assume the species are perfectly mixed, and use the average concentrations as the initial values and neglect the diffusion effect in the y direction. In this case, no matter how the species premix, they have the same average concentration and the model will produce the same result. In practice, species are rarely uniformly mixed in microsystems.[13]

To capture the real behavior of the reactive fluid in microreactors, we discretize our system and use multiple PFRs to model the microreactor. The discretization in the y direction allows the use of many small parallel PFRs. As a result, the variation of the inlet concentration to each discretized PFR is small, and the error produced by the assumption of perfect mixing is decreased. To calculate the diffusional mixing in the y direction, we also need to discretize the system in the x direction.

PFR Combination Model. We first introduce what we will call the PFR combination model. Here, we separate the system in the x direction into two stages as shown in Figure 3. The first stage is a column of small PFRs in parallel, and the second stage is a full width PFR. The total volume of the PFRs remains the same as the original micro reactor. After the fluid flows out of the column of parallel PFRs, we mix the streams, giving the average concentration of all the flows for the input concentration to the full width PFR. This perfect mixing we enforced at the end of the first stage approximates the overall diffusional mixing effect inside of the reactor. There are two discretization parameters in this model: the number of parallel PFRs in the first stage, and the length ratio of the parallel PFRs to the full width PFR. Generally speaking, a large number of parallel PFRs reduces the error produced by an initial assumption of perfect mixing. The length ratio decides the position at which the perfect mixing takes place. These two parameters vary for systems having different Pe and Da. For modeling a system with known results, we may tune the PFR combination model by adjusting the two discretization parameters to minimize the approximation error. Figure 4a shows the model behavior for a system with $Pe = 20$, and $Da = 1$. In this case, the mixing efficiency at the reactor inlet is fixed. As an example, we may use two parallel PFRs in the first part and tune the model by changing the length ratio. From the figure, we can see that this model with the length ratio around 0.9 produces an accurate result. Figure 4b shows the good agreement between the known results, and the model results for different mixing efficiencies at the reactor inlet. The match of the results shows the possibility to use mul-

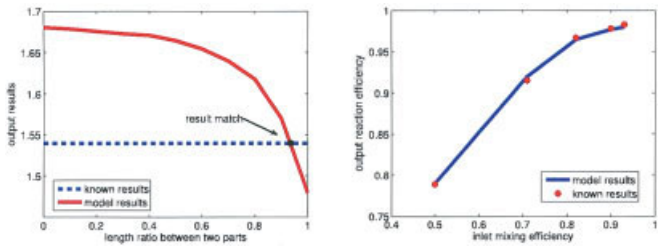

Figure 4. Results from the PFR combination model.

(Left) (a) Tune the model to produce an accurate result; (right) (b) comparison between COMSOL and Matlab results. [Color figure can be viewed in the online issue, which is available at www.interscience.wiley.com.]

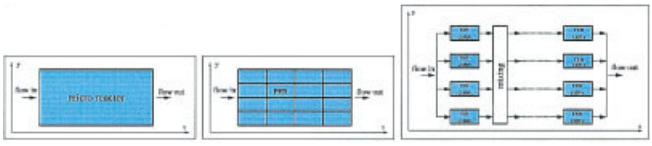

(a) Micro reactor (b) Discretization (c) Calculation

Figure 5. The microreactor is represented by a PFR network model. The calculation of reaction and convection is conducted in one column of PFRs and the calculation of diffusional mixing is conducted between two columns of PFRs.

[Color figure can be viewed in the online issue, which is available at www.interscience.wiley.com.]

tiple PFRs for modeling a microreactor. However, to effectively use this model for design, we need to know *a priori* how to discretize the system more precisely; we need a function to decide the values of the two discretization parameters for the given *Pe* and *Da*. We have found no general approach to identifying such a function. Still, we believe the idea of using a network of PFRs to emulate our microchannel reaction system has merit.

PFR Network Model. In the previous PFR combination model, we mix the fluids perfectly after they flow out from the first part. However, the flow mechanism for mixing in the y direction is caused only by diffusion which is rarely perfect. In our second PFR network model, the discretization in the x direction is modified to allow the calculation of diffusional mixing in the y direction. The PFR network as shown in Figure 5, which still maintains the same total reactor volume, is used to model our system. This network has M rows and N columns. Each PFR in the network has the length of l, and the width of w. We use $P_{m,n}$ to stand for the small PFR in the mth row and nth column. The concentrations of the species inside $P_{m,n}$ can be represented as a vector $\mathbf{C}_{m,n}(x) = [c^A_{m,n}(x),\ c^B_{m,n}(x),\ c^T_{m,n}(x),\ c^{AT}_{m,n}(x),\ c^{BT}_{m,n}(x)]$, where the range of x is from 0 to l. In this PFR network model, the calculation of concentration change is conducted alternatively in the x and y direction.

Step 1: Equation 7 is used to calculate convection and reaction inside each PFR in the first column to generate $\mathbf{C}_{m,1}(x)$. The initial values $\mathbf{C}_{m,1}(0)$ are the discretized concentrations made by assuming perfect mixing at the inlet of each small reactor.

Step 2: Calculate the average concentration $\overline{\mathbf{C}_{m,1}}$ inside each PFR. This average concentration is used in the next step for approximating the diffusional mixing.

Step 3: Fick's second diffusion law is used in the y direction between two columns of PFRs to approximate the concentration change caused by the diffusional mixing. We approximate the second derivative with finite difference

$$\Delta\mathbf{C}_{m,1} = D \cdot \frac{\overline{\mathbf{C}_{m-1,1}} - 2\overline{\mathbf{C}_{m,1}} + \overline{\mathbf{C}_{m+1,1}}}{w^2} \cdot \frac{l}{v} \tag{8}$$

Step 4: Calculate the inlet concentrations for the PFRs in the second column

$$\mathbf{C}_{m,2}(0) = \mathbf{C}_{m,1}(l) + \Delta\mathbf{C}_{m,1} \tag{9}$$

Then the calculation will repeat from *Step 1* to *Step 4* until reaching the final column. The combination of the two parameters M and N that produces accurate results for a system with given Pe and Da is not unique. A fine mesh can lead to a result with certain accuracy, but requires long computational time.

Comparison of the PFR Based Model. The two models in this section are developed based on the PFR design equation. The spatial discretization decoupled the physical phenomena in the system: reaction, convection, and diffusion. These models are physically intuitive and properly capture the fluid behavior in the system. Table 1 shows a brief summary of the characteristics of the two models. The PFR combination model can always produce an accurate result, but the rule for conducting the discretization is hard to generate. The PFR network model is less accurate than the PFR combination model, since the two discretization parameters have to be integers. However, it has a simpler discretization rule. In general, accuracy is improved by increasing the number of PFRs in the network. Some exceptions exist, they are discussed in more detail in the "Model Verification" Section.

MOL Model. In this section, we develop the microreactor model using the numerical method of lines, which is a technique for solving partial-differential equations by discretizing all, but one dimension, and then integrating the semidiscrete problem as a system of ODEs.[36] We discretize the system in the y direction and apply MOL to calculate the effects of diffusion in the y direction. The original set of PDEs is reformulated into a set of ODEs as follows

$$v_{ix}\frac{\partial c_i^m}{\partial x} = D_i\left(\frac{c_i^{m-1} - 2c_i^m + c_i^{m+1}}{\Delta y^2}\right) + r_i \tag{10}$$

where m stands for the mth discretization in the y direction, Δy is the discretized channel width. Increasing the amount of discretization results in higher accuracy but longer computation time. This set of ODEs can readily be solved by a standard ODE solver.

Model verification. To verify the accuracy of our models, we developed a partial-differential equation based model using finite element methods in FEMLAB, and compared the results with our discretized PFR network model and MOL model.

Table 1. The Characteristics of the Two PFR Based Models

Characteristics		PFR Network Model	PFR Combination Model
Discretization	Channel width	M: # of PFRs	M: # of PFRs
	Channel length	r: Length ratio of the two parts	N: # of PFRs
Mixing	Position	Between the two parts	Between columns of PFRs
	Mechanism	Complete mixing	Fick's 2nd law of diffusion
Reaction and convection		PFR design equation	PFR Design equation

Table 2. Comparison Between Three Models

Models		Results for Decreasing Mesh Size					
FEMLAB Model	Error (%)	0.0	0.4	4.7	8.2	9.9	25
	Time (s)	545	321	161	78.5	24.5	14.5
PFR Network Model	Error (%)	2.7	4.1	4.5	5.8	18	47
	Time (s)	2.38	1.0	0.38	0.32	0.18	0.16
MOL Model	Error (%)	1.1	1.5	1.7	3.4	6.0	21
	Time (s)	12.1	1.0	0.38	0.14	0.12	0.11

Table 2 shows the comparison of the model accuracy and the computation time.[1] For the FEMLAB model, we first generated a grid independent solution, which is listed in the first column. This solution needs a long calculation time. We consider it accurate, and use it as the basis for comparison. Using a coarser mesh shortens the computation time, but at the expense of accuracy. We also change the amount of discretization for the PFR network model, and the MOL model to characterize their accuracy and efficiency. Table 2 shows that both the PFR network model and the MOL model produce accurate results and have substantially shorter computation time than the FEMLAB model.

The MOL model is highly stable. Increasing the discretization always improves the result accuracy. Our experience tells us that it normally takes less than one second to produce an adequately accurate result. The PFR network model was observed to become numerical unstable when very fine mesh are used. Varying the discretization in the x and y direction sometimes leads to an inaccurate or even an infeasible solution. Even though the instability can be identified and avoided by using several different model discretizations and repeating the calculation, this instability makes this approach unsuitable for iterative model evaluation-based design.

The model analysis and example results in the following sections are based on the MOL model.

Model Analysis

When designing a micro reactor, we aim to produce high-product yields and selectivities, and there are many parameters that will affect the design results. The most important of these parameters include the reactor geometry, physiochemical properties, and reaction kinetics. For a given set of parameters, our model can produce the accurate results. However, to ensure a good design, we need to understand how these parameters affect product yields and selectivities. Here, we use the model to identify the parametric sensitivity for a specific example.

We consider a competitive tagging reaction system, which is often employed in immunoassay design.[6] This system has two reversible reactions

$$A + T \underset{k_2}{\overset{k_1}{\rightleftharpoons}} AT \tag{11}$$

$$B + T \underset{k_4}{\overset{k_3}{\rightleftharpoons}} BT \tag{12}$$

[1] Results obtained by a AMD Athlon XP 1700+, 768MB RAM.

where T stands for the molecular tag in this system. A and B are the molecules we seek to tag for subsequent identification; typically proteins, DNA sequences, or nucleic acids. They compete to react with T. In the reaction system shown in Figure 2, A and B are first introduced into the well 1, and T into the well 2. When a suitable set of voltages applied in the reservoirs, species A, B, and T are introduced into the reaction channel, where they undergo two second-order reversible reaction processes to produce AT and BT. This reaction system has forward, second-order rate constants of k_1 and k_3, and reverse, first-order rate constants of k_2 and k_4. The reaction term r_i in Eq. 10 can be expressed as

$$r_i = \begin{cases} -k_1 c_A c_T + k_2 c_{AT} & i = A \\ -k_1 c_B c_T + k_2 c_{BT} & i = B \\ -k_1 c_A c_T - k_3 c_B c_T + k_2 c_{AT} + k_4 c_{BT} & i = T \\ k_1 c_A c_T - k_2 c_{AT} & i = AT \\ k_3 c_B c_T - k_4 c_{BT} & i = BT \end{cases} \tag{13}$$

In this system, there are twenty parameters and seven variables as shown in Table 3. By using the Buckingham π theorem, we can relate the concentration variables with the reactant conversion and the product yield. The original twenty parameters are reduced to fifteen dimensionless parameters. The reformulation procedure and the final results are listed in Table 4. Here α_i, β_i, λ_i, and γ_j are the scaling parameters; τ is the ratio of the convection time to the diffusion time for A, and Da is the Damkohler number based on the properties of species A

$$\tau = \frac{L}{PeW} = \frac{D_A L^2}{\mu_A V W^2} \tag{14}$$

$$Da = \frac{C_{A0} k_1 L^2}{\mu_A V} \tag{15}$$

Table 3. Twenty Original Parameters and Variables for the Example Micromixing-Reaction System

Parameters	Diffusivity	$D_i \quad i = A, B, T, AT, BT$
	Mobility	$\mu_i \quad i = A, B, T, AT, BT$
	Initial concentration	$C_{i0} \quad i = A, B, T$
	Kinetic constant	$k_j \quad j = 1, 2, 3, 4$
	Electric potential gradient	V
	Reaction channel length	L
	Reaction channel width	W
	Concentration	$c_i \quad i = A, B, T, AT, BT$
Variables	Position along channel length	x
	Position along channel width	y

Table 4. Using Buckingham π Theorem to Formulate the Dimensionless Parameters and Variables

	Intermediate Formulation	Dimensionless Formulation
Parameters	$D_A,\ \alpha_1 D_A,\ \alpha_2 D_A,\ \alpha_3 D_A,\ \alpha_4 D_A$	$\alpha_i \quad i = 1, 2, 3, 4$
	$\mu_A,\ \beta_1\mu_A,\ \beta_2\mu_A,\ \beta_3\mu_A,\ \beta_4\mu_A$	$\beta_i \quad i = 1, 2, 3, 4$
	$C_{A0},\ \lambda_1 C_{A0},\ \lambda_2 C_{A0}$	$\lambda_i \quad i = 1, 2$
	$k_1,\ \gamma_1 C_{A0} k_1,\ \gamma_2 k_1,\ \gamma_3 C_{A0} k_1,$	$\gamma_j \quad j = 1, 2, 3$
	V	τ
	L	Da
	W	
Variables	$\frac{c_A}{C_{A0}}, \frac{c_B}{C_{B0}}, \frac{c_T}{C_{T0}}, \frac{c_{AT}\mu_{AT}}{C_{T0}\mu_T}, \frac{c_{BT}\mu_{BT}}{C_{T0}\mu_T}$	$X_p,\ Y_q,\ p = A, B, T \quad q = AT, BT$
	$\frac{x}{L}$	ϕ
	$\frac{y}{W}$	ξ

After the reformulation, the physical meanings of the dimensionless variables are: $X_p = 1 - conversion\ of\ reactant\ p$ and $Y_q = yield\ of\ product\ q$. Using these dimensionless parameters and variables, the PDEs in Eq. 10 can be rewritten as

$$\frac{\partial X_A}{\partial \phi} = \tau\left(\frac{\partial^2 X_A}{\partial \xi^2}\right) - Da\lambda_2 X_A X_T + \frac{\gamma_1\lambda_2\beta_2 Da}{\beta_3} Y_{AT} \quad (16)$$

$$\frac{\partial X_B}{\partial \phi} = \frac{\alpha_1\tau}{\beta_1}\left(\frac{\partial^2 X_B}{\partial \xi^2}\right) - \frac{\gamma_2 Da\lambda_2}{\beta_1} X_B X_T + \frac{\gamma_3\lambda_2\beta_2 Da}{\beta_1\lambda_1\beta_4} Y_{BT} \quad (17)$$

$$\frac{\partial X_T}{\partial \phi} = \frac{\alpha_2\tau}{\beta_2}\left(\frac{\partial^2 X_T}{\partial \xi^2}\right) - \frac{Da}{\beta_2} X_A X_T - \frac{\gamma_2 Da\lambda_1}{\beta_2} X_B X_T + \frac{\gamma_1 Da}{\beta_3} Y_{AT} + \frac{\gamma_3 Da}{\beta_4} Y_{BT} \quad (18)$$

$$\frac{\partial Y_{AT}}{\partial \phi} = \frac{\alpha_3\tau}{\beta_3}\left(\frac{\partial^2 Y_{AT}}{\partial \xi^2}\right) + \frac{Da}{\beta_2} X_A X_T - \frac{\gamma_1 Da}{\beta_3} Y_{AT} \quad (19)$$

$$\frac{\partial Y_{BT}}{\partial \phi} = \frac{\alpha_4\tau}{\beta_4}\left(\frac{\partial^2 Y_{BT}}{\partial \xi^2}\right) + \frac{\gamma_2 Da\lambda_1}{\beta_2} X_B X_T - \frac{\gamma_3 Da}{\beta_4} Y_{BT} \quad (20)$$

Then we use the model described in the "MOL Model" section, to solve this set of PDEs and perform the sensitivity analysis. Here, we define three categories to classify these parameters: sensitive parameters, conditionally sensitive parameters, and insensitive parameters. For sensitive parameters, changing their values will produce obvious variation of product yields and selectivities. For insensitive parameters, variation of their values barely change the final results. The behavior of a conditionally sensitive parameter relies on the values of some other parameters. It can be sensitive if the requirements for some other parameters' values are satisfied; otherwise, it will be insensitive. Table 5 shows how the fifteen dimensionless parameters fit into the three categories.

Table 5. Parametric Sensitivities

Sensitive parameters	$Da,\ \beta_2,\ \gamma_1,\ \gamma_2,\ \lambda_2$
Conditionally sensitive parameters	$\alpha_1,\ \beta_1,\ \beta_3,\ \beta_4,\ \gamma_3,\ \lambda_1$
Insensitive parameters	$\tau,\ \alpha_2,\ \alpha_3,\ \alpha_4$

Sensitive parameters

Da, β_2, γ_1, γ_2, and λ_2 are sensitive parameters. When designing a microreactor, we need to put emphasis on this category. Having a control of these parameters can lead to a good design. Figure 6 shows one example result of the sensitive parameters. γ_2 is related to the forward rate of the second reaction. When it is increased, the second reaction extent is also increased and more T reacts with B to produce BT. As a result, the yield and selectivity of AT is decreased.

Conditionally sensitive parameters

α_1, β_1, β_3, β_4, γ_3, and λ_1 are conditional-sensitive parameters. α_1, β_1, and λ_1 are the parameters related to the reactant B in the second reaction. These three parameters can be sensitive when the second reaction has a comparable reaction rate with the first one. Figure 7 shows the example results for the parameter β_1. β_3 and β_4 are parameters related to the reaction product AT and BT. When Da is large, which means the first reaction is fast and enough AT is produced, β_3 is sensitive. For β_4, it also requires that the second reaction has a comparable

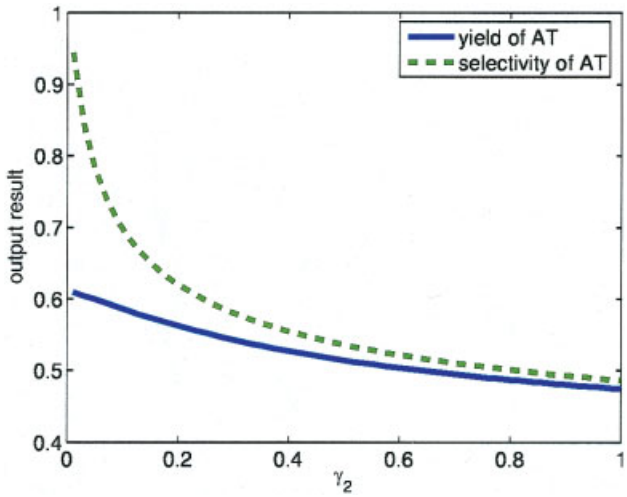

Figure 6. The variation of product yield and selectivity with γ_2.

[Color figure can be viewed in the online issue, which is available at www.interscience.wiley.com.]

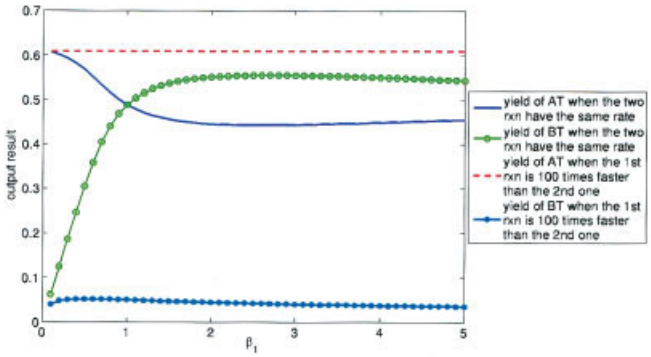

Figure 7. The variation of product yield and selectivity with β_1.

[Color figure can be viewed in the online issue, which is available at www.interscience.wiley.com.]

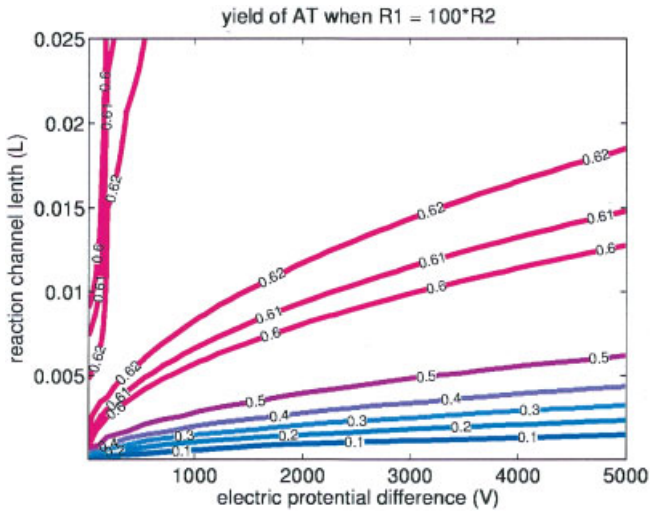

Figure 8. Contour plot of the dependence of product yield on the reactor channel length and the electric potential difference. The number on each curve is the value of product yield.

[Color figure can be viewed in the online issue, which is available at www.interscience.wiley.com.]

reaction rate with the first reaction. γ_3 is related to the second reaction's backward kinetic constant. It is sensitive when the second reaction is not slow and enough BT is produced. When those conditions are satisfied, change the values of the conditional sensitive parameters will change the product yields and selectivities.

Insensitive parameters

τ, α_2, α_3, and α_4 are nonsensitive parameters. Variation of these parameters do not significantly change the output.

Example Results

After the parametric sensitivity analysis, we now use our models for microreactor design. Our design objectives are to increase the yield and selectivity of the desired product, and to decrease the reactor size and computation time. We consider the same reaction system as described by Eq. 11 and 12. For competitive immunoassay,[6] the two reactions normally have the same reaction speed. Here, as a contrast example, we choose $k1 = 100k3$, assuming the first reaction is much faster than the second one, and AT is the desired product of the system. Thus, we can find out how the sensitivity of parameter affects the yield and selectivity of the desired product. The physiochemical properties of the species are listed in Table 6.

From the sensitivity analysis in the previous section, we know that product yields and selectivities are sensitive to Da. In a reactive microfluidic reactive system, the chemical properties of reactants and products and the reaction kinetic constants are fixed. From the Eq. 15, we can see that the remaining sensitive design variables are the reactor channel length and the electrokinetic potential difference.

Figures 8 and 9 are two contour plots showing the dependence of product yield and selectivity on the reactor channel length and the electric potential difference. When designing a system with a given set of voltage, the contour plots can help to decide how long the reactor channel length should be to achieve a certain product yield or selectivity. When we have a system with a given reactor channel length, we can also use the model to find out the appropriate voltage difference that needs to be applied for the system.

For this reaction system, the desired product is AT. We want to increase the yield and selectivity of AT. The two contour plots show the trade off between the yield and the selectivity. Suppose we have a system with a fixed voltage of 3,000 V, and a very short reaction channel with the length of 0.002 m, Figure 9 shows that in this system the selectivity of AT is close to one. However, the equivalent point in Figure 8 indicates that the yield of AT is close to zero, because the species don't have enough residence time for reaction. Increasing the reactor channel length increases the residence time. More AT is produced, and the yield of AT is increased. Since the second reaction is much slower than the first one, the longer residence time does not increase the production of BT and the resulting amount of BT is still limited. As a result, the selectivity of AT is also increased. If we continue to increase the reactor channel length until it reaches a certain value, the residence time can be long enough that the first reaction reaches equilibrium and the yield becomes constant. However, the second reaction is still far from equilibrium and the long residence time continues to increase the production of BT. As a result, the selectivity of AT is decreased. For the system with a fixed reactor channel length, we observe the similar procedure when decreasing the electric-potential difference. By using our model, we can vary the channel reactor length and the set of voltages applied to the wells to achieve an optimized design that maximizes the

Table 6. Physiochemical Properties of Species

	A	*B*	*T*	*AT*	*BT*
μ (m^2/V s)	2.84e-8	2.84e-8	4.45e-8	3.5e-8	3.5e-8
D (m^2/s)	3.3e-10	3.3e-10	1e-10	2e-10	2e-10

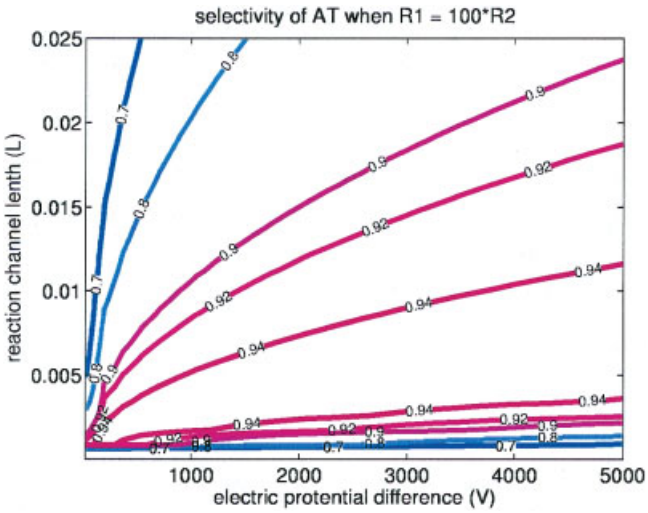

Figure 9. Contour plot of the dependence of product selectivity on the reactor channel length and the electric potential difference. The number on each curve is the value of product selectivity.

[Color figure can be viewed in the online issue, which is available at www.interscience.wiley.com.]

amount of *AT* produced without mixing it with the byproduct *BT*, and minimizes the reactor channel length.

One curve in the contour plots represents the same value for the product yield in Figure 8, and the product selectivity in Figure 9, which indicates that when changing the reactor channel length, and the electric potential difference simultaneously by a certain ratio, the product yield and selectivity can be maintained as constant. Since all the curves start from the left lower corner, all the product yields and selectivities can be found at the left lower corner in these two figures. This characteristic of the two figures shows that using the model calculation results, we can achieve the high-yield and selectivity by applying a short reactor channel and a low-electric potential difference, which results in the minimized reactor size and decreased energy cost.

Conclusions

In this article, we presented two models for microfluidic mixing-reaction systems that are driven by electroosmosis. The first model is based on the network of PFR. It improves the understanding of physical phenomena in a reactive microfluidic system. The second model employs MOL, which has the advantage of easy implementation and simple calculation. Both models use discretization methods to convert the PDE system into an ODE system. The models are validated against a COMSOL PDE model and shown to be accurate and fast. The models can take in arbitrarily mixed concentration profiles and model the systems with different operational conditions, such as channel length or electric potential difference. The example results show that the models can be used to design a microfluidic mixing-reaction system. These microreactor models can be combined with models for other LoC subsystems to build the LoC design methodology.

Acknowledgment

This research effort is sponsored by the Defense Advanced Research Projects Agency (DARPA) and U. S. Air Force Research Laboratory under agreement number F30602-01-2-0987, and by the National Science Foundation (NSF) under award CCR-0325344. The authors would like to thank members of the SYNBIOSYS group at Carnegie Mellon University.

Literature Cited

1. Reyes DR, Iossifidis D, Auroux A, Manz A. Micro total analysis systems. 1. Introduction, theory and technology. *Anal Chem.* 2002;74:2623–2634.
2. Chow AW. Lab-on-a-chip: Opportunities for chemical engineering. *AICHE J.* 2002;48(8):1590–1595.
3. Auroux A, Iossifidis D, Reyes DR, and Manz A. Micro total analysis systems. 2. Analytical standard operations and applications. *Anal Chem.* 2002;74:2637–2652.
4. Hempel G. Biomedical applications of capillary electrophoresis. *Clin Chem Lab Med.* 2003;41(6):720–723.
5. Lee G, Chen S, Huang G, Sung W, Lin Y. Microfabricated plasitic chips by hot embossing methods and their applications for dna separation and detection. *Sen Actuators B.* 2001;75:142–148.
6. Chiem NH, Harrison DJ. Microchip systems for immunoassay: an integrated immunoreactor with electrophoretic separation for serum theophyllone determination. *Clin Chem.* 1998;44(3):591–598.
7. Su F, Chakrabarty K. Architectural-level synthesis of digital microfluidics-based biochips. In *Proceedings of International Conference on Computer Aided Design,* p 223–228. IEEE; Nov: 2004.
8. Ehrfeld W, Hessel V, Lehr H. *Microreactors: New Technology for Modern Chemistry.* Wiley-VCH; 2000.
9. Pfeiffer AJ, Mukherjee T, Hauan S. Simultaneous design and placement of multiplexed chemical processing systems on microchips. In *Proceeding of ICCAD 2004,* pages 229–236. IEEE; 2004.
10. Kahng AB, Măndoiu I, Reda S, Xu X, Zelikovsky AZ. Evaluation of placement techniques for dna probe array layout. In *ICCAD '03,* pages 262–269: November; 2003.
11. Harrison DJ, Skinner C, Cheng SB. From Micro-Motors to Micro-Fluidics. In: *International Conference on Solid-State Sensors and Actuators.* pages 40–44; 1997.
12. Wang Y, Magargle R, Lin Q, Hoburg J, Mukherjee T. System-oriented modeling and simulation of biofluidic lab-on-a-chip. In: *Proceedings of TRANSDUCERS '05.* pages 1280–1283; 2005.
13. Wang Y, Lin Q, Mukherjee T. Analytical models for complex electrokinetic passive mixers. In: *Micro Total Analysis Systems (MicroTAS 2004),* pages 596–598; 2004.
14. Wang Y, Lin Q, Mukherjee T. System-oriented dispersion models of general-shaped electrophoresis microchannels. *Lab-on-a-chip.* 2004;4:453–463.
15. Magargle R, Hoburg JF, Mukherjee T. Microfluidic injector models based on neural networks. In: *Proceedings of NanoTech (MSM '05),* pages 616–619; 2005.
16. Jacobson SC, Hergenroder R, Koutny LB, Warmack RJ, and Ramsey JM. Effects of injection schemes and column geometry on the performance of microchip electrophoresis devices. *Anal Chem.* 1994;66:1107–1113.
17. Culbertson CT, Jacobson SC, and Ramsey JM. Dispersion sources for compact geometries on microchips. *Anal Chem.* 1998;70:3781–3789.
18. Jensen KF. Microsystems for chemistry and energy applications. In: *Semiconductor Device Research Symposium,* 2001; pages 418–421.
19. Haswell SJ, Middleton RJ, O'Sullivan B, Skelton V, Watts P, Stying P. The application of microreactors to synthetic chemistry. *Chem Commun.* 2001;5:319–398.
20. Ajmera SK, Delattre C, Schmidt MA, Jensen KF. Microfabricated differential reactor for heterogenous gas phase catalyst testing. *J Catal.* 2002;209:401–412.
21. Fletcher PDI, Haswell SJ, Paunov VN. Theoretical considerations of chemical reactions in micro-reactors operating under electroosmotic and electrophoretic control. *Analyst.* 1999;124:1273–1282.
22. Haswell SJ, Watts P. Green chemistry: Synthesis in microreactors. *Green Chem.* 2003;5:240–249.
23. Vlachos DG. Stochastic modeling of chemical microreactors with detailed kinetics—induction times and ignitions of H2 in air. *Chem Eng Sci.* 1998;53(1):157–168.

24. Chatterjee AN, Aluru NR. Combined circuit/device modeling and simulation of integrated microfluidic systems. *J of Micro Electro Mechanical Systems.* 2005;14(1):81–95.
25. MacInnes JM, Du X, and Allen RWK. Dynamics of electroosmotic switching of reacting microfluidic flows. *Trans IChemE.* 2003;81:773–786.
26. Harries N, Burns JR, Barrow DA, Ramshaw C. A numerical model for segmented flow in a microreactor. *Int J Heat Mass Transfer.* 2003;46: 3313–3322.
27. Pfeiffer AJ. Synthesis of multiplexed biofluidic microchips. *In press for IEEE transactions on Computer-Aided Design of Integrated Circuits and Systems: Special Issue on design automation tools for microfluidic-based biochips;* 2005.
28. Losey MW, Jackman RJ, Firebaugh SL, Schmidt MA, Jensen KF. Design and fabrication of microfluidic devices for multiphase mixing and reaction. *J Microelectromech Sys.* 2002;11(6):709–717.
29. Probstein RF. *Physiochemical Hydrodynamics: An Introduction.* 2 ed. Wiley & Sons; 1994.
30. MacInnes JM. Computation of reacting electrokinetic flow in microchannel geometries. *Chem Eng Sci.* 2002;57:4539–4558.
31. Harmon BJ, Patterson DH, Regnier FE. Mathematical treatment of electrophoretically mediated microanalysis. *Anal Chem.* 1993;65: 2655–2662.
32. Cummings EB, Griffiths SK, Nilson RH, Paul PH. Conditions of similitude between the fluid velocity and electric field in electroosmotic flow. *Anal Chem.* 2000;72:2526–2532.
33. Bird RB, Stewart WE, Lightfoot EN. *Transport Phenomena.* 2nd ed. John Wiley and Sons; 2001.
34. Fogler HS. *Chemical reaction engineering.* 3rd ed. Prentice Hall; 1999.
35. Patankar NA, Hu HH. Numerical simulation of electroosmotic flow. *Anal Chem.* 1998;70:1870–1881.
36. Schiesser WE. *The Numerical Method of Lines: Integration of Partial Differential Equations.* Academic Press, Inc.; 1991.

Manuscript received Dec. 16, 2005, and revision received Jun. 8, 2006.